Iraqi Journal of Science, 2025, Vol. 66, No. 2, pp: 890-900
DOI: 10.24996/ijs.2025.66.2.26

ISSN: 0067-2904

Multi-Classification Brain Tumor by Mixed Transform with ResNet34

Rasha Ali Dihin
Department of Computer Science, Faculty of Education for Women, University of Kufa, Najaf, Iraq.

Received: 24/9/2023 Accepted: 10/6/2024 Published: 28/2/2025

Abstract

Brain tumors pose a significant global health concern, imposing substantial social and economic burdens. Accurate classification of tumor types (gliomas, meningiomas, and pituitary tumors) from MRI data is essential for aiding radiologists and avoiding invasive biopsies. This paper presents a new method for brain tumor classification that has excellent accuracy when compared with existing methods. The proposed method provides improvements for feature extraction and classification. This new method comprises MRI image preprocessing, feature extraction, and image classification. Preprocessing includes resizing and data augmentation. Following this, features are extracted from MRI images using a mixed transform approach involving a mix of methods like DWT (Discrete Wavelet Transform), FAN (FAN Transform), and DCT (Discrete Cosine Transform). Classification employs the ResNet34 model. Where the outcomes demonstrate a training accuracy of 0.9439, a validation accuracy of 0.9195, and a best accuracy of 0.9397 when distinguishing between different brain tumor tissues in MRI images.

Keywords: Tumors, DWT, ResNet34, MRI, FAN

تصنيف متعدد لأورام الدماغ بواسطة التحويل المختلط مع*ResNet34*

رشا علي دهن

قسم علوم الحاسبات, كلية التربية للبنات, جامعة الكوفة, النجف الاشرف, العراق

الخلاصة

تشكل أورام الدماغ مصدر قلق صحي عالمي كبير، وتفرض أعباء اجتماعية واقتصادية كبيرة. يعد التصنيف الدقيق لأنواع الأورام (الأورام الدبقية، والورم السحائي، وأورام الغدة النخامية) من بيانات التصوير بالرنين المغناطيسي أمرًا ضروريًا لمساعدة أطباء الأشعة وتجنب الخزعات الغازية. تقدم هذه الورقة إطارًا آليًا مبتكرًا يشتمل على المعالجة المسبقة لصور الرنين المغناطيسي واستخراج الميزات وتصنيف الصور. تتضمن المعالجة المسبقة تغيير الحجم وزيادة البيانات. وبعد ذلك، يتم استخراج الميزات من صور التصوير بالرنين المغناطيسي باستعمال نهج تحويل مختلط يتضمن مزيجًا من الأساليب مثل DWT (تحويل المويجات المنفصلة)، وFAN (تحويل FAN)، وDCT (تحويل جيب التمام المنفصل). يستعمل التصنيف نموذج ResNet34. حيث توضح النتائج دقة التدريب 0.9439، ودقة التحقق من الصحة 0.9195، وأفضل دقة 0.9397 عند التمييز بين أنسجة ورم الدماغ المختلفة لصور الرنين المغناطيسي.

* Email: rashaa.aljabry@uokufa.edu.iq

1. Introduction

Brain tumors represent a profoundly devastating affliction affecting the human body today. These tumors can emerge across diverse regions of the brain, often revealing symptoms only at later stages, posing a significant threat to life.
Symptoms of brain disorders can include difficulties in hearing or speaking, recurrent headaches, memory deficits, declining vision, and alterations in one's personality [1].

In 2016, brain tumors ranked as the leading cause of cancer-related deaths in children aged 0–14 in the United States, surpassing leukemia. Brain and Central Nervous System (CNS) tumors also rank as the third most prevalent cancer among teenagers and adolescents aged 15–39. Distinct medical interventions are necessary for various brain tumor types [2].

As per the redefined World Health Organization (WHO) classification from 2016, a brain tumor pertains to abnormal growths impacting the central nervous system, where the technique used is the use of molecular genetics with histological classification that is based on tissues and their characteristics. Generally, brain tumors encompass an aberrant proliferation of brain cells, leading to size reduction and significant damage to the neural network, thereby disrupting brain function. Two primary categories of brain tumors, akin to cancer, exist: cancerous (malignant) and non-cancerous (benign). Predominant brain tumor types, based on their location, include meningioma, glioma, and pituitary tumors. The levels of cancer in each type vary. Gliomas grow in glial tissues and the spinal cord, meningiomas grow in the protective membrane, and pituitary tumors grow in the pituitary gland [3].

Early brain tumor detection is vital for accurate diagnosis and is often facilitated through magnetic resonance imaging (MRI), a non-invasive technique providing sensitive tissue contrast. MRI's capacity to accommodate normalized tissue aids in visualizing structures of interest within human brain tumors. Swift intervention is essential to prevent the tumor from affecting adjacent brain tissues [4]. To enhance radiologists' diagnostic accuracy, diverse techniques have been proposed, with deep learning standing out. Deep learning autonomously learns increasingly complex features from data, yielding impressive outcomes in medical diagnosis and disease classification, elevating accuracy [5].

Deep learning is a subset of machine learning that empowers computers to predict and draw conclusions from data by acquiring the ability to comprehend data representations. These methods are notably harnessed for medical image classification and serve as a prominent avenue within computational intelligence techniques. Despite achieving remarkable success across a wide range of applications in various domains, deep learning approaches have the inherent challenge of being data-hungry, requiring at least tenfold the number of data samples to flex their learning capacity. To overcome the constraint of limited training data, transfer learning emerges as a solution by adapting previously acquired knowledge from a similar problem. Transfer learning involves training a network on a large dataset (the base dataset) and subsequently transferring this acquired knowledge to a smaller dataset (the target dataset) [6].

2.Related work

Numerous approaches have been presented for automated brain MRI classification utilizing deep learning. Several research studies employing deep learning techniques have been conducted to tackle challenges related to binary and multiclass brain tumor diagnosis.

Vankdothu and Hameed [1] Introducing a novel automated approach for the detection and classification of brain disorders. This methodology is organized into discrete stages, including preprocessing of MRI images, segmentation of images, extraction of relevant features, and image categorization. In this method, the IKMC algorithm, which is an improvement to the K-means clustering algorithm, was used in the segmentation image stage, while in the feature extraction stage, gray-level co-occurrence was used. In the final stage of the method, deep learning was used for the final classification. The classification categories include four categories: gliomas, meningiomas, and non-cancerous cases. Tumors, tumors of the pituitary gland. The accuracy achieved by applying the model to the Kaggle dataset was 95.17%.

Neelum et al. [4] suggested a model that combines machine learning and deep learning models to automatically classify brain tumors. In the feature extraction stage, two deep learning models were used: Xception and Inception-v3. While in the classification stage, machine learning methods (SVM), (KNN), and (RF) were used. The accuracy for classification when merging Xception with KNN, SVM, and RF was 93.79, while the accuracy when merging with Inception-v3 reached 94.34%.

Palash et al. [5] introduced a new model, SE-ResNet-101, that is based on merging the squeeze and excitation blocks with ResNet-101. In the pre-processing stage, normalization and zero-centering were used to increase the data. Then, in the feature extraction and classification stage, the ResNet-101 model was used, and the classification accuracy of the model without using data augmentation techniques was 89.93%, while when using data augmentation techniques, it improved the classification accuracy to 93.83%.

Sonavane et al. [7] present an innovative approach for the classification of brain tumors using 2D convolutional neural networks. The study introduces denoising and normalization as an initial step in image preprocessing. The proposed methodology consists of three sequential stages: In the first stage, image smoothing with a smooth filter and an anisotropic diffusion filter is applied to reduce noise. The second stage focuses on the extraction of features from brain MRI images using 2D CNN. For the third stage, the classification of MRI images into malignant or benign categories was carried out using the SVM algorithm. The experimental validation encompassed the utilization of MRI images, culminating in an overall accuracy of 80%.

Cheng et al. [8] evaluated the brain tumor classification performance through the implementation of Region of Interest (ROI) augmentation and a refined ring-form partition technique. These enhancements were integrated with various feature extraction methods, including intensity histogram, GLCM, and the Bag-of-Words (BoW) approach. The resulting feature vectors were then input into a classifier. The experimental results demonstrated accuracy improvements, increasing from 71.39% to 78.18% for intensity histogram, from 83.54% to 87.54% for GLCM, and from 89.72% to 91.28% for BoW.

3. Proposed Methodology

The proposed methodology encompasses three distinct phases, outlined as follows: preprocessing and augmentation comprise the initial stage, feature extraction constitutes the second stage, and classification concludes the third phase. Figure 1 provides a detailed description of each step.

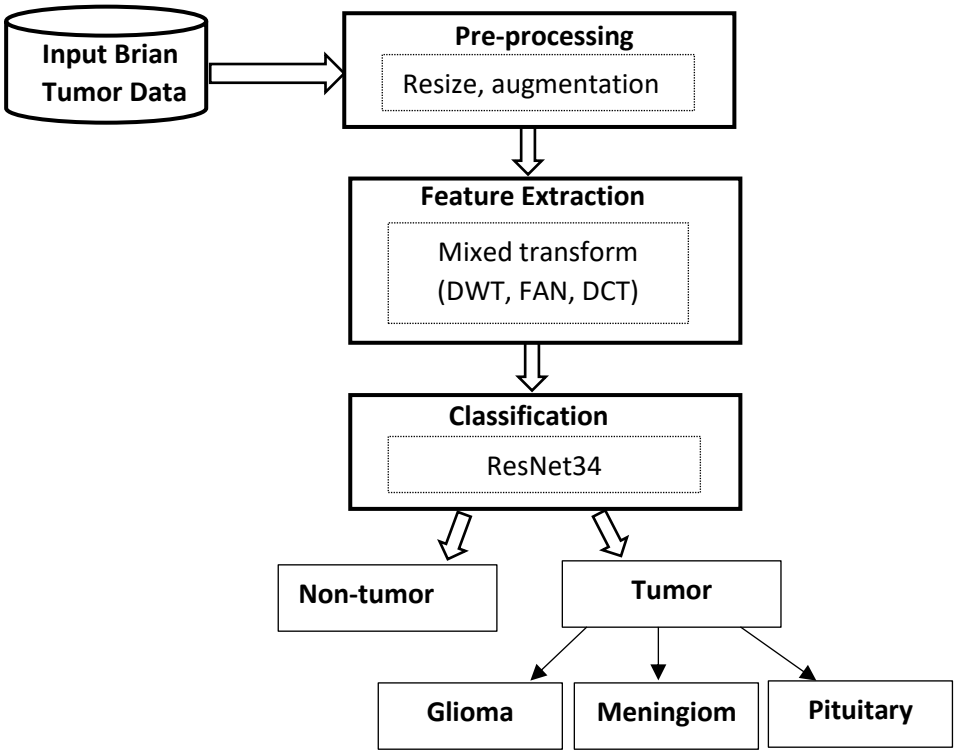

Figure 1: Proposed methodology overview.

3.1. Proposed architecture

The structure of the proposed approach is outlined in three main segments: preprocessing, feature extraction, and classification. The elaboration of each step is presented in comprehensive detail below.

A. Image Resize

In the prepressing stage, the input image was resized to (224 x 224) to standardize the size of the input image.

B. Data augmentation

Serves as an additional form of regularization, mitigating model overfitting by expanding the training dataset through manipulation of existing original information. The concept of data augmentation is longstanding, with diverse techniques applied across various problems [9].

Common transformations like flipping and rotation (e.g., 45 to 90 degrees) along with variable-degree shear operations are employed as a framework for this purpose.

C. Feature Extraction

For image feature extraction, a substantial range of image intensity levels are utilized as input. Here, we used mixed transforms from DCT, FAN, and DWT. These cascading transformations have an effect on input signals. The initial transformation typically shifts the signal from the time domain to the frequency domain. However, this presents an issue for applying subsequent transformations, as the signal is already in the frequency domain after the first transformation. To address this, a solution is needed. Hybrid transformations utilize the FAN transform, which scrambles the frequency domain while preserving information. This enables the next transformation to be applied by mitigating the conflict that arises from the signal being in the frequency domain. These transformations convert the image into multiple frequency bands, which will provide a multi-resolution analysis.

This transformation can allow a CNN to focus on different aspects of the data, such as local and global features, textures, and edges. This can lead to a more accurate and meaningful representation of features.

3.2 Discrete Wavelet Transform (DWT)

The wavelet transform (WT) is a mathematical method employed in signal analysis within signal processing, utilizing orthogonal waves. It has found recent application in diverse areas like noise reduction and pressure analysis [10]. The core idea of wavelet transformation is to represent any function as a combination of waves, with wavelets serving as localized time-frequency functions. This allows you to capture local features in the frequency domain while simultaneously extracting information from the time and frequency domains. The discrete wavelet transform (DWT) dissects data into distinct components across different frequency ranges, aiding image processing by accommodating separate data. In digital image processing, the 2D-DWT transforms input images into sets of low- and high-frequency information, including vertical, horizontal, or diagonal orientations [11]. We used DWT because we will transform the image from the time domain to the frequency domain, thus obtaining more accurate details. More than one transformation was mixed because the first transformation (DCT) transformed the image from the time domain to the frequency domain and was used for DWT to convert the image to the time domain.

In this case, we will have a problem applying the DWT transformation because it usually transforms the image from the time domain to the frequency domain. Therefore, the second transformation cannot be applied directly. Therefore, transform mixed the FAN transform that was used to solve this problem because this conversion mixes the frequency domain, but it still preserves all the information.

While additional transformations can be charged computational power, the benefits you discover from them as they become better features and more powerful models may outweigh this cost and can capture different features of the input data, such as low-frequency and high-frequency components. It can help prevent damage to the devices during the extra time, but applying these transformations reduces the dimensions of the input data (taken from the input image), which in turn reduces the training time for the CNN.

3.3 FAN Transform

FAN introduces image scrambling encryption. Theory utilizing the Arnold transform broadens the range of transform matrices from a singular type to an infinite variety, termed the FAN transform set. Although the FAN transform also exhibits periodicity, its infinite transform set renders direct decryption impossible without knowledge of the applied transform matrices. Moreover, FAN transform sets encompass a substantial range, allowing even a few transformations to yield significant enhancements. The following provides a definition of the FAN transform set: Given the overall expression for the N-order square transformation of images, we establish the FAN transform collection in the following manner [12]:

$$\begin{pmatrix} r1' \\ r2' \end{pmatrix} = \begin{pmatrix} t_{11} & t_{12} \\ t_{21} & t_{22} \end{pmatrix} \begin{pmatrix} r1 \\ r2 \end{pmatrix} mod\ N - r1, r2 \in \{0,1,2, \ldots . N-1\} \quad (1)$$

$t11 \times t22 - t12 \times t21 = \pm 1$

The Eq. (1) in the FAN transform is readily encountered. In the Arnold transformation, when we have t11 = 1, t12 = 1, t21 = 1, and t22 = 2, then the condition 1 * t22 - t12 * t21 = ±1

is fulfilled. This scenario aligns with the FAN transform's evolving conditions, representing a distinct case within the FAN transform framework.
Here, (r1, r2) represents the pixel coordinates in the original image, and (r1', r2') represents the coordinates of the pixels in the transformed new image. The digital image's matrix, N, denotes its size, which is typically a square [13].

3.4 Discrete Cosine Transform (DCT)

The Discrete Cosine Transform (DCT) is employed to produce a finite sequence resembling cosine functions oscillating at different frequencies. It acts as a means to break down any signal into its fundamental frequency constituents [14]. Operating in a block-based manner, the DCT partitions an image or frame into non-overlapping blocks of size N × N. Given an input image X and an output image Y (with dimensions N × M), the DCT coefficients are computed according to Eq. (2) [15].

$$Y(u1,v1) = \left(\frac{2}{r1}\right)^{\frac{1}{2}} \left(\frac{2}{r2}\right)^{\frac{1}{2}} \alpha \sum_{r1=0}^{R1-1} \sum_{r2}^{R2-1} X(r1,r2) \cos\frac{(2r1+1)}{2r1} \cos\frac{(2r2-1)v1\pi}{2r2} \quad (2)$$

$$\alpha = \frac{1}{\sqrt{2}} \quad for\ u1,v1 = 0$$

$$\alpha = 1 \quad for\ u1,v1 = 1,2,\ldots.M-1$$

$$\sum_{r1=0}^{R1-1} \sum_{r2}^{R2-1} X(r1,r2)$$

The DCT serves to depict a signal using a minimal set of coefficients, whereas the DFT presents a periodic portrayal of the signal through coefficient truncation.
The algorithm for applying mixed transforms (DWT, FAN, and DCT)

Input: Image X
Output: Transformed image Z

Step 1: Apply the Discrete Wavelet Transform (DWT)
1. Compute the DWT of the image X to obtain matrix Y.

Step 2: Apply of FAN Transform
1. Initialize K = 0. // constant for save the maximum of the absolute value of the coefficients
2. For each coefficient a_ij in Y:
   a. Update K = Max (K, ABS(a_ij)).
3. Create an empty matrix r.
4. For each coefficient a_ij in Y:
   Compute r_ij = a_11 / (a_00 * a_11 - a_01 * a_10) for r_00.
   Compute r_ij = -a_01 / (a_00 * a_11 - a_01 * a_10) for r_01.
   Compute r_ij = -a_10 / (a_00 * a_11 - a_01 * a_10) for r_10.
   Compute r_ij = a_00 / (a_00 * a_11 - a_01 * a_10) for r_11.
   Append [r_ij] to the corresponding row in matrix r.
5. For each position (i, j) in Y:
   Apply the scrambling expression using K and matrix R to modify Y (i, j).

Step 3: Apply the Discrete Cosine Transform (DCT)
Compute the DCT of the modified matrix Y to obtain the final transformed matrix Z.
Output Z as the transformed image.

D. Classification using ResNet34

The classification procedure was employed to categorize each image according to its distinctive features. Classification is considered a basic process for distinguishing between normal brain images and diseased brain images, as it includes the process of assigning elements within a group to specific categories or levels [16], [17]. Accurately predicting the target category for each data point is the main goal of classification. By adding the ResNet34 model, the method of image classification can be improved. Actively using the ResNet34 model to classify brain tumors was the primary goal of this work. The images on which this transformation has been applied and features extracted will be input to ResNet34 for further processing.

ResNet34 can generalize better to unseen data and different types of input as the network learns more diverse representations and focuses on specific frequencies to improve feature extraction.

4. Experimental Results

A. Dataset

In this work, the proposed model was tested on the Kaggle dataset, as this evidence included four types of disease, namely glioma tumors, meningioma tumors, pituitary tumors, and normal cases. The data was divided into two categories, namely the training set, which amounted to 2870 images. While the test group contained 394 images. To improve data representation, various data preprocessing techniques, including brain stripping, were applied. The performance evaluation was carried out across four classes: glioma tumors, meningioma tumors, instances with no tumors, and pituitary tumors.

Data set source:

https://www.kaggle.com/sartajbhuvaji/brain-tumor-classification-mri.

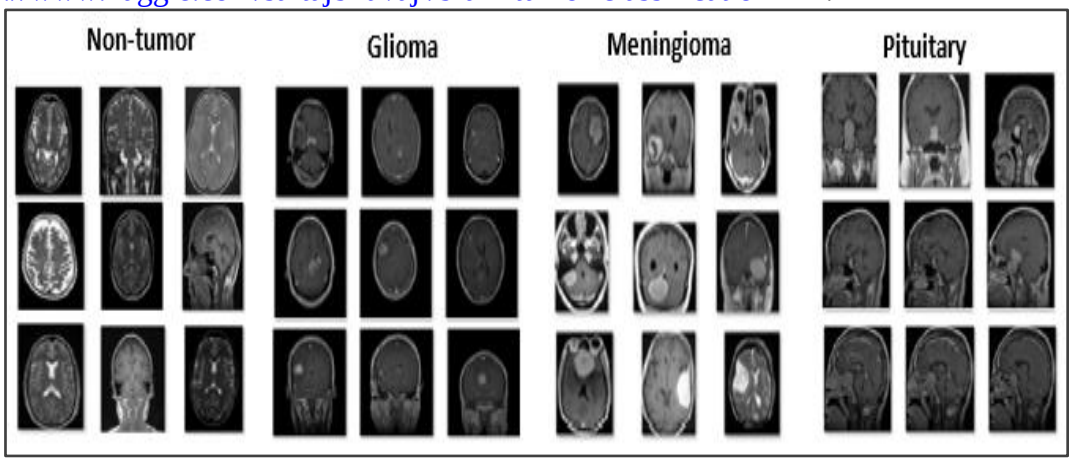

Figure 2: Sample Brain tumor MRI Images.

B. Evaluation Parameters

The evaluation of the brain tumor classification model's performance was carried out using a range of classification evaluation metrics. Multiple performance indicators, such as accuracy, specificity, sensitivity, and F1-Score, were utilized for assessment [18], [19].

$$ACC = \frac{TP+TN}{TP+TN+FP+FN} \quad (3)$$

$$SE = \frac{TP}{TP+FN} \quad (4)$$

$$SP = \frac{TN}{FP+TN} \quad (5)$$

$$F1\ Score = 2.\frac{Precision \times Recall}{(Precision+Recall)} \quad (6)$$

C. Implementation

As previously detailed, we conducted testing of the neural network using the Kaggle dataset. Table 1 shows the results of training and testing, with an achieved accuracy of 0.9667%, accompanied by a validation accuracy of 0.9631%. The training loss was measured at 0.4521, while the validation loss was 0.4601, and the highest accuracy recorded during training was 0.9686%. This remarkable level of consistency was attained during the 100th epoch of training. Employing an image size of 224x224 and the cancerous brain database, we utilized the ResNet34 model with a mixed transformer for feature extraction. In Figure 3, we present the classification results for multiple classes, which include accuracy and loss values. The results in Figure 4 of the input samples of a brain MRI display in (a), (b), (c), and a resultant class of the proposed method are shown in (d), (e), and (f), respectively.

Table 1: Accuracy and loss of model over 100 epochs

Epochs	Train-loss	Train-Acc.	Val-loss	Val-Acc.	Best -Acc.
1/100	0.7461	0.7990	0.6897	0.8506	
10/100	0.6324	0.8518	0.5867	0.8707	
20/100	0.5987	0.8760	0.6082	0.8736	
30/100	0.5763	0.9047	0.5440	0.9023	
40/100	0.5539	0.9213	0.5161	0.9195	0.9686
50/100	0.5288	0.9255	0.5081	0.9224	
60/100	0.5142	0.9365	0.5292	0.9382	
70/100	0.5058	0.9458	0.4987	0.9395	
80/100	0.4904	0.9599	0.4929	0.9487	
90/100	0.4703	0.9662	0.4740	0.9594	
100/100	0.4521	0.9667	0.4601	0.9631	

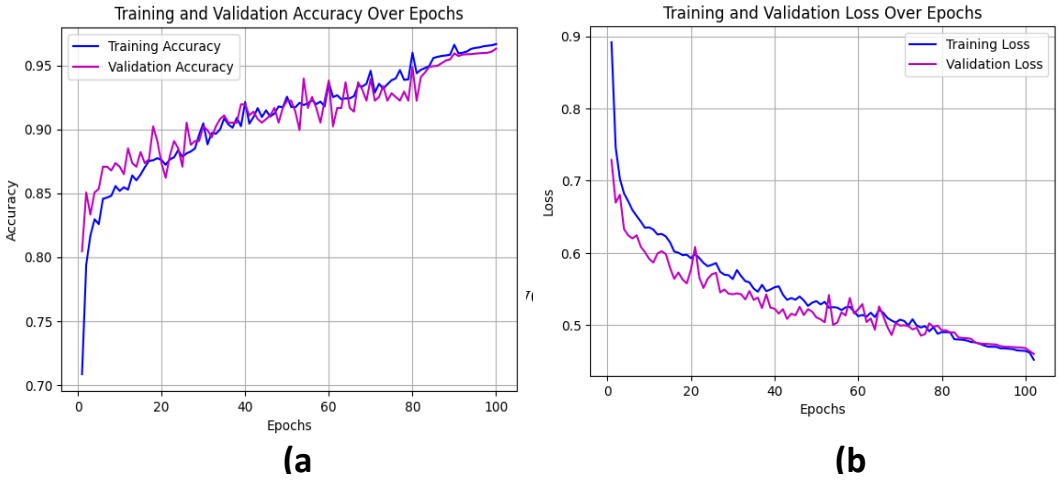

Figure 3: Training and validation over 100 epochs, (a) accuracy, (b) loss

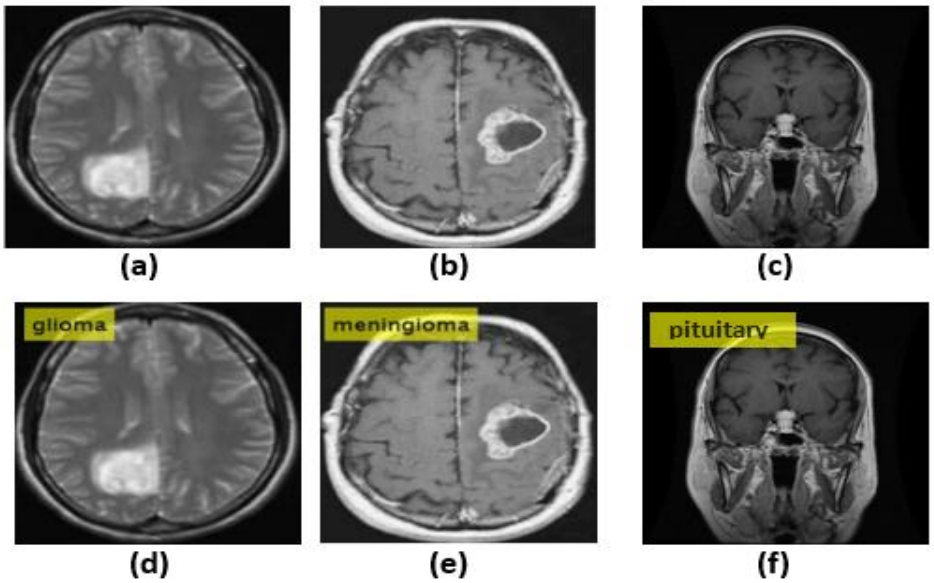

Figure 4: Analysis of the Classification (a) (b) (c) Input Image; (d) (e) (f) Output Classified Image.

Table 2 shows the accuracy metrics that are extracted from the confusion matrices. The model achieves the highest performance in precision, sensitivity, specificity, F1-score, and accuracy. Within Table 2, you will discover accuracy metrics derived from the confusion matrices, highlighting the model's exceptional performance. These metrics encompass precision, sensitivity, specificity, F1-score, and accuracy. For feature extraction, the model in question uses ResNet34 with a mixed transformer. When it comes to classifying brain tumors, it deals with multiple classes.

Table 2: Performance Evaluation of Models

Tumor type	Sensitivity	Specificity	F1_Score	Accuracy
No-tumor	0.9798	0.9850	0.9841	99%
Glioma-tumor	0.6666	0.9801	0.9170	95%
Meningioma-tumor	0.9310	0.9186	0.9552	97%
Pituitary-tumor	0.6117	0.9936	0.8641	94%
Average	0.7972	0.9693	0.9301	96.25%

Figure 5 presents the confusion matrix, which provides a summary of the system's performance. On the X-axis, it represents the predicted values, and on the Y-axis, it shows the true labels.

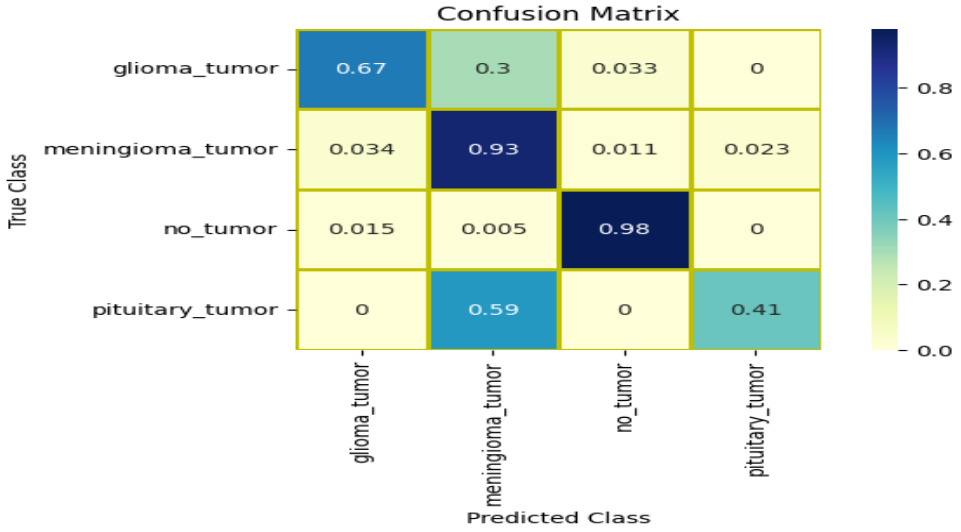

Figure 5: Confusion matrix of model

Table 3: Comparison between the proposed and existing models

Author (Ref.)	Method	Proposed Solution and Preprocessing Approach	Evaluation
Vankdothu. R. and Hameed. M.A [1]	Recurrent RCNN	Improved K-means clustering (IKMC)was used for segmentation stage, the gray level co-occurrence matrix (GLCM) was used for feature extraction stage, then RCNN model to classify the MRI images	Test accuracy= 95.17%
Neelum Noreen et al. [4]	Inception-v3	the use of a group of techniques such as SVM, RF, KNN, and SoftMax.	94.34%
Palash Ghosal et al. [5]	SE-ResNet-101	Squeeze and Excitation blocks merged with ResNet-101	93.83%
Himar Fabelo et al. [7]	2D-CNN	Smooth filter to denoise and 2D-CNN with SVM	80%
Cheng, Jun, et al. [8]	BoW model	Dilation used as the ROI and used bag-of-words for feature extraction	91.28%
Pawel Mlynarskia et al. [20]	DL- mixed supervision	Deep Learning Fully-Annotated and Weakly-Annotated	85.67%
Proposed Method	Mixed T - ResNet34	Used mixed transform with ResNet34 for feature extraction and classification	96.25%

4. Conclusion

In this proposed method, we have presented a model that can automatically recognize the three most common types of brain tumors: pituitary, glioblastoma, and meningioma. Our proposed method is divided into three main sections: data preprocessing and feature extraction from MRI images using a transformation technique. Mixed and final image classification using the ResNet34 architecture. Experiments were conducted on the Kaggle dataset in order to evaluate the effectiveness of our proposed method. The model achieves an amazing accuracy of 0.9439 during training, while in the testing phase the accuracy was 90% and the sensitivity was 0.7163, while the F1 score reached 0.9525. These results demonstrate the success of our proposed method in correctly classifying different types of brain tumors.

References

[1] R. Vankdothu and M. A. Hameed, "Brain tumor MRI images identification and classification based on the recurrent convolutional neural network," *Measurement: Sensors*, vol. 24 p. 100412, 2022, Doi: 10.1016/j.measen.2022.100412.

[2] N. Saranya, D. Karthika Renuka and J. N. Kanthan, "Brain tumor classification using convolution neural network," *Journal of Physics Conference Series*, vol. 1916, no. 1, pp. 012206, 2021, doi:10.1088/1742-6596/1916/1/012206

[3] A. M. Alqudah, H. Alquraan, A. Qasmieh, A. Alqudah, and W. Al-Sharu, "Brain tumor classification using deep learning technique -A comparison between cropped, uncropped, and segmented lesion images with different sizes," *International Journal of Advanced Trends in Computer Science and Engineering* , vol. 8, no. 6, pp. 3684–3691, 2019, Doi: 10.30534/ijatcse/2019/155862019.

[4] N. Noreen, S. Palaniappan, A. Qayyum, I. Ahmad, and M. Alassafi, "Brain Tumor Classification Based on Fine-Tuned Models and the Ensemble Method," Computers, *Materials and Continua*, vol. 67, no. 3, pp. 3967–3982, 2021, Doi: 10.32604/cmc.2021.014158.

[5] P. Ghosal, L. Nandanwar, S. Kanchan, A. Bhadra, J. Chakraborty, and D. Nandi, "Brain tumor classification using ResNet-101 based squeeze and excitation deep neural network," *In 2019 Second International Conference on Advanced Computational and Communication Paradigms*

(ICACCP) IEEE, 2019, Doi: 10.1109/ICACCP.2019.8882973.

[6] A. Rehman, S. Naz, M. Razzak, F. Akram, and M. Imran, "A Deep Learning-Based Framework for Automatic Brain Tumors Classification Using Transfer Learning," *Circuits, Systems, and Signal Processing*, vol. 39, no. 2, pp. 757–775, 2020, Doi: 10.1007/s00034-019-01246-3.

[7] H. Fabelo, M. Halicek, S. Ortega, M. Shahedi, A. Szolna, J.F. Piñeiro, and M. Márquez, "Deep learning-based framework for in vivo identification of glioblastoma tumor using hyperspectral images of human brain," *Sensors* , vol. 19, no. 4, 2019, Doi: https://doi.org/10.3390/s19040920.

[8] J. Cheng, W. Yang, M. Huang, W. Huang, J. Jiang, Y. Zhou, R. Yang, J. Zhao, Y. Feng, Q. Feng, and W. Chen, ''Retrieval of brain tumors by adaptive spatial pooling and Fisher vector representation,'' *PLoS ONE*, vol. 10, no. 10, p. e0140381, 2015, Doi: 10.1371/journal.pone.0140381.

[9] A. Naseer, T. Yasir, A. Azhar, T. Shakeel, and K. Zafar, "Computer-Aided Brain Tumor Diagnosis: Performance Evaluation of Deep Learner CNN Using Augmented Brain MRI," *International Journal of Biomedical Imaging*, vol. 2021, p. 5513500, 11, 2021. https://doi.org/10.1155/2021/5513500

[10] Y. Liu, L. Guan, C. Hou, H. Han, Z. Liu, Y. Sun, and M. Zheng, "Wind Power Short-Term Prediction Based on LSTM and Discrete Wavelet Transform," *Applied Sciences*, vol. 9, no. 2, pp. 1108-1115, Mar. 2019. Doi: 10.3390/app9061108.

[11] J. Nobre and R. F. Neves, "Combining Principal Component Analysis, Discrete Wavelet Transform and XGBoost to trade in the financial markets," *Expert Systems with Applications*, vol. 125, pp. 181–194, Jul. 2019. Doi: 10.1016/j.eswa.2019.01.083.

[12] L. Honglian and F. Jing, "Generalization of Arnold transform—FAN transform and its application in image scrambling encryption," *Recent Advances in CSIE, LNEE,* vol. 128, pp. 511–516, 2012.

[13] N. Jiang, W. Wu, and L. Wang, " The quantum realization of Arnold and Fibonacci image scrambling," *Quantum information processing*, vol. 13, no.5, pp. 1223-1236, 2014.

[14] S. S. Sawant and P. Manoharan, "Unsupervised band selection based on weighted information entropy and 3D discrete cosine transform for hyperspectral image classification," *International Journal of Remote Sensing*, vol. 41,no. 10, pp. 3948–3969, 2020. Doi: 10.1080/01431161.2019.1711242.

[15] Z. Zhao, J. Zhang, S. Xu, Z. Lin, and H. Pfister, "Discrete Cosine Transform Network for Guided Depth Map Super-Resolution," *In Proceedings of the IEEE/CVF Conference on Computer Vision and Pattern Recognition*, 2022, pp. 5687–5697. Doi: 10.1109/CVPR52688.2022.00561.

[16] F. J. Díaz-Pernas, M. Martínez-Zarzuela, M. Antón-Rodríguez and D. González-Ortega ''A Deep Learning Approach for Brain Tumor Classification and Segmentation Using a Multiscale Convolutional Neural Network," *Healthcare (Basel, Switzerland)*, vol. 9, no. 2, p. 153, Feb. 2021, doi:10.3390/healthcare9020153

[17] L. Zhang, Y. Bian, P. Jiang, and F. Zhang, "A Transfer Residual Neural Network Based on ResNet-50 for Detection of Steel Surface Defects," *Applied Sciences*, vol. 13, no. 9, pp. 5260-5278, 2023. Doi: 10.3390/app13095260.

[18] J. Kang, Z. Ullah, and J. Gwak, "MRI-based brain tumor classification using ensemble of deep features and machine learning classifiers," *Sensors*, vol. 21, no. 6,p. 2222, 2021. Doi: 10.3390/s21062222.

[19] H. H. Sultan, N. M. Salem, and W. Al-Atabany, "Multi-Classification of Brain Tumor Images Using Deep Neural Network," *IEEE Access*, vol. 7, pp. 69215-69225, 2019.

[20] P. Mlynarski, H. Delingette, A. Criminisi, and N. Ayache "Deep Learning with Mixed Supervision for Brain Tumor Segmentation," *arXiv*, vol. 6, no. 3, 2018, Doi: 10.1117/1.JMI.6.3.034002.